EXPERIMENTS AT CCRS USING ERS TANDEM MODE DATA

A.L. Gray, K.E. Mattar[1], D. Geudtner[2], P.W. Vachon

Canada Centre for Remote Sensing, 588 Booth St., Ottawa, Ontario, K1A 0Y7

phone: (613) 995-3671, fax: (613) 947-1383,

email: laurence.gray ccrs.nrcan.gc.ca

ABSTRACT

ERS tandem mode data has been used in a number of interferometric SAR experiments at the Canada Centre for Remote Sensing (CCRS). In this paper, results from two experiments will be described, one related to Arctic terrain mapping and propagation problems, and the other to the measurement of ice movement in a temperate glacier in the Canadian Rockies.

1. INTRODUCTION

In the first experiment we selected a test site on Bathurst Island to evaluate the potential for ERS tandem mission and Radarsat repeat-pass interferometric synthetic aperture radar (InSAR) for DEM generation and scene coherence estimation of Arctic terrain. This is appropriate for repeat-track interferometry because of the desert nature of the terrain (between our data acquisitions there was minimal snow accumulation) and because the low atmospheric water vapour content would minimise propagation inhomogeneities. Successful interferometric pairs were obtained with all the tandem mode data studied and also with RADARSAT 24 day repeat data. As well as the satellite data, high quality airborne cross-track InSAR data was collected using the CCRS CV-580 C-band mapping radar. From this data we have assembled a radar mosaic (~35 x 180 km) of the eastern half of Bathurst data and a digital elevation model with a height noise in the 1 to 3 m rms for most of the radar swath, but increasing to around 4-5 m rms at the swath edge. Height bias errors were minimised by using the sea ice surrounding Bathurst Island. This data is sufficiently accurate to use as a reference data set against which to evaluate the results of the satellite InSAR mapping experiment.

In the second experiment, ERS tandem mode image pairs were used to track ice movement of the Saskatchewan Glacier in the Canadian Rockies. This glacier is very accessible and the results of the experiment have been compared with good historical data and with in-situ ice movements obtained by traditional glaciological techniques.

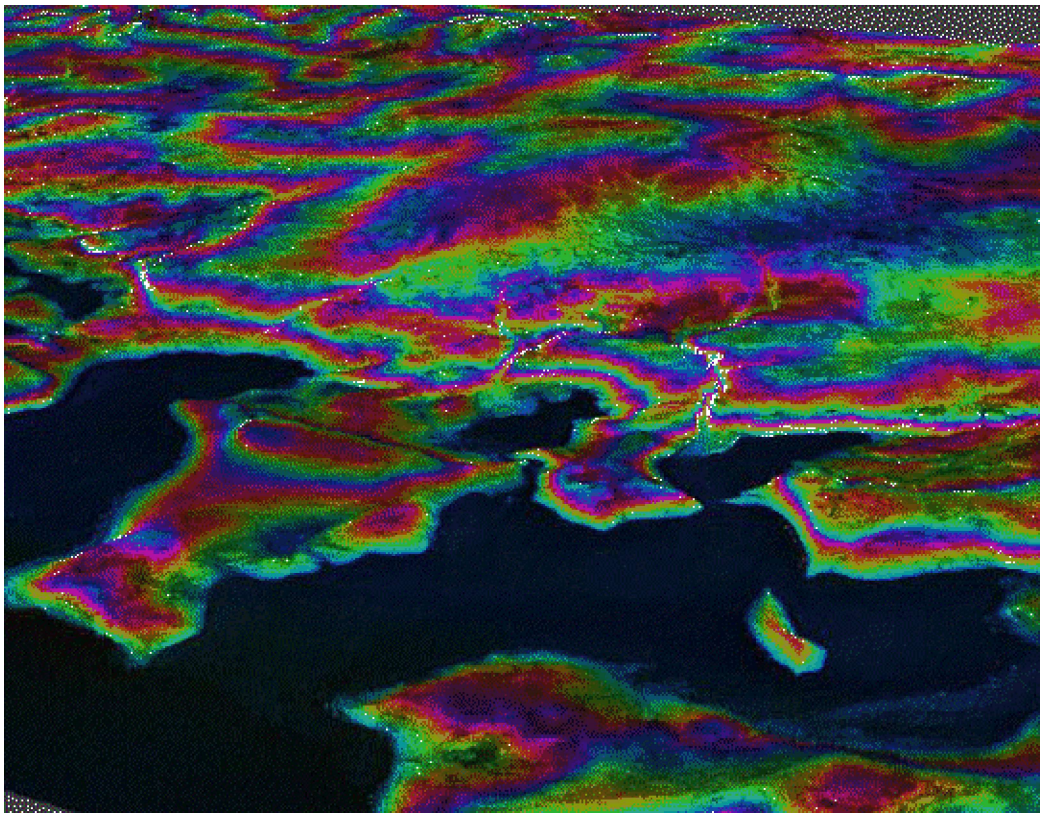

Figure 1: Perspective view of Bathurst island test site, viewed from the south-westerly direction, was obtained from a CV-580 InSAR derived DTM. Each colour cycle represents a 50 m change in elevation. The data was acquired April, 1995. The sea, visible in the foreground, was frozen at the time.

For both test sites precise ERS orbit data generated by GFZ Potsdam (Massmann et al., 1993) and digital elevation models (DEMs) obtained from the CCRS airborne interferometric SAR (InSAR) system were used. The ERS interferometric imaging geometry was reconstructed using the accurate orbit data which, together with the airborne InSAR DEM, allowed the calculation of the expected slant range interferogram from the tandem pair. By forming the product of the predicted interferogram with the complex conjugate of the actual interferogram, the influence of topography can be removed and information related to ground movement, or atmospheric propagation inhomogeneities, is observed in the residual phase. For the Arctic test sites results will be shown for 4 tandem mode pairs and the non-uniformity of the differential phase is explained in terms of residual propagation inhomogeneities. Phase errors in the range of 1 to 2 radians on scales of 1 to 10's of km were observed. These phase errors appear not to be related to errors in the digital terrain model or orbit knowledge and may impact the accuracy of terrain movement estimation and of extracted topography, depending on the baseline.

Saskatchewan Glacier movement has been the focus of previous studies (Vachon et al., 1996) in which 5 pairs of ascending pass ERS tandem mode data were used to satisfactorily measure the glacier's flow rate, as validated by in situ point surveying measurements. In this work, we extend the data set to also consider the descending passes in an attempt to obtain a more accurate flow field determination. However, it is now evident that the descending pass geometry is worse (the projection of the

motion vector along the radar line of site for the descending passes is small and leads to a less accurate estimate). Even two observations with different geometry's are not adequate to solve for the 3-D flow field.

2. ARCTIC EXPERIMENT

A perspective view of our test site on Bathurst island of the Canadian arctic, generated from an accurate digital terrain model (DTM) by CV-580 InSAR system, is shown in Figure 1. The barren, rocky, wind-swept, vegetation free terrain ensured high coherence for the ERS tandem interferometry repeat pass experiment. Four similar tandem pairs, all ascending and all with the same relative orbit (RO) were selected. These are detailed in Table 1.

The ERS interferometric processing used is described in detail elsewhere (Geudtner, 1995). Basically, the SLC images were first co-registered using a cross-correlation analysis. The images were then filtered in range and azimuth. The range filtering selects only overlapping portions of the object spectrum based on a spectral analysis of the interferogram to determine the fringe frequency. The azimuth filtering suppresses non-overlapping portions of the azimuth Doppler spectra resulting from processing with different Doppler centroid frequencies. The filtered images were then oversampled by a factor of two in both range and azimuth, and the interferogram was formed. The coherence is then estimated using an averaging window size of 50 (azimuth) by 10 (range) samples and corrected for finite signal-to-noise ratio. Since the azimuth and range filtering avoid decorrelation due to spectral misalignment and the measured coherence has been corrected for finite signal-to-noise ratio, the resulting coherence estimate may be interpreted as the temporal scene coherence. The scene coherence for the four tandem pairs considered here are shown in Figure 2. The scene coherence in all cases is very high except for the dark pattern which correlate well with the drainage network, where isolation from the wind results in snow accumulation or changes in the snow crystalline structure.

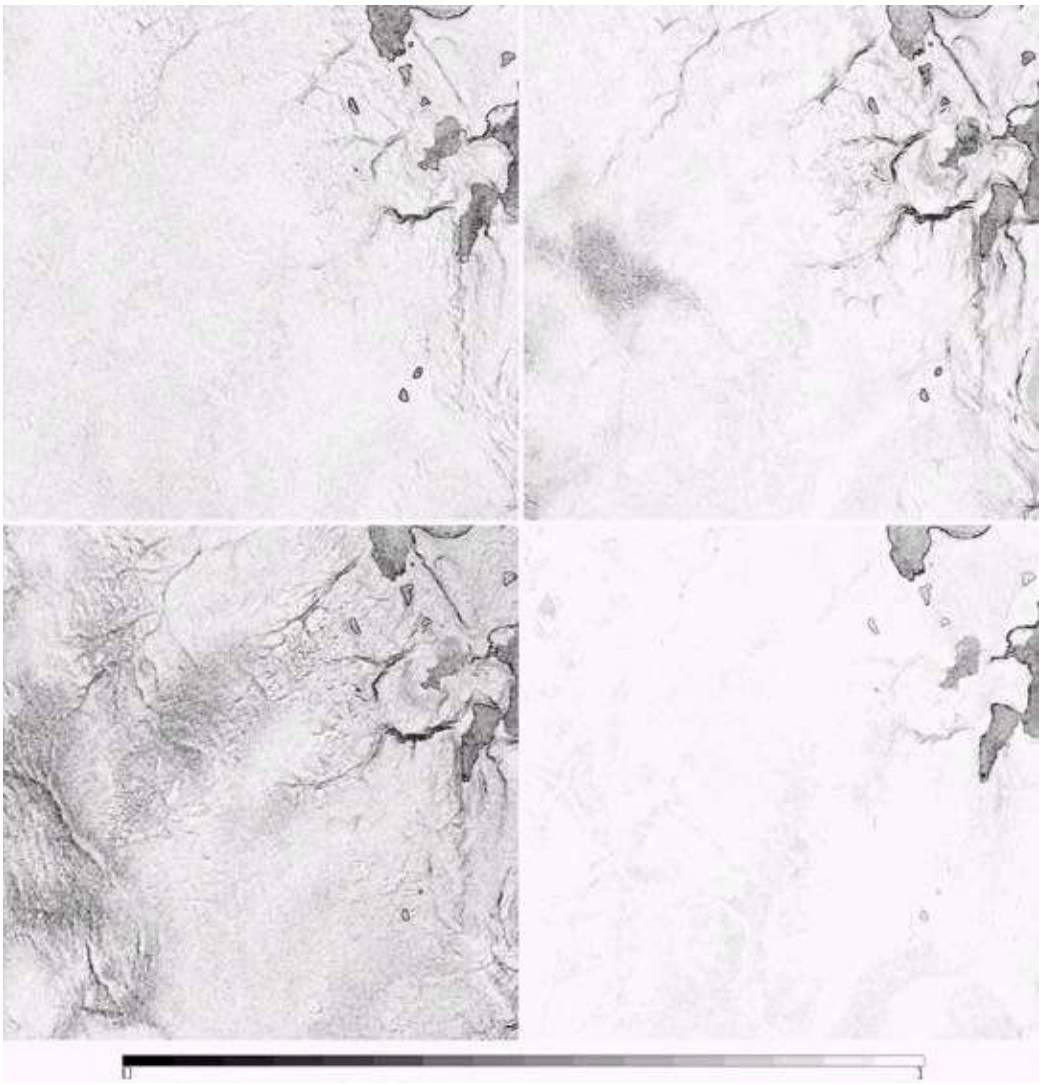

Figure 2: Set of scene coherence maps from the ERS tandem mode interferograms of Bathurst island. The time sequence is from upper left to lower right and follows the sequence in Table 1.

Pass Date	Orbit	RO	B_n (m)
Jan 3/4, 1996	23367/3694	333	120
Feb 7/8, 1996	23868/4195	333	191
Mar 13/14, 1996	24369/4696	333	183
Apr 17/18, 1996	24870/5633	333	63

Table 1: Summary of ascending passes of ERS-1/2 data over Bathurst Island

The interferogram phase is given by:

$$\phi_{int} = \phi_{top} + \phi_{disp} + \phi_{atm} + \phi_{noise}, \quad (1)$$

where ϕ_{top} is the component of the phase due to topography:

$$\phi_{top} = 4\pi B_n \Delta h / \lambda R_1 \sin\theta, \quad (2)$$

where B_n is the normal component of the baseline, Δh and θ the incidence angle. ϕ_{disp} is the component of the phase due to displacement of the footprint on the ground. It can be expressed as:

$$\phi_{disp} = \delta B\, 4\pi / \lambda = V_{los}\, \delta t\, 4\pi / \lambda, \quad (3)$$

where δB is the displacement, λ is the wavelength, V_{los} is the line-of-site velocity of the object on the ground covered by the footprint, and δt is the time interval. ϕ_{atm} is the component of the phase due to extraneous atmospheric propagation effects, and ϕ_{noise} other noise sources such as scene decorrelation.

We make use of the digital terrain model (DTM) derived from the CV-580 InSAR system (Mattar et al., 1994,) to remove the topographic component from the interferogram phase. With the use of the precise orbit data, PRC, supplied by D-PAF (Massmann et al., 1993), and using a modification of the algorithm described by Geudtner & Schwäbisch (1996), we project the DTM from UTM co-ordinates into phase in the ERS-1 slant range perspective. We then manually optimise the registration between the ERS interferogram and the synthetic interferogram, in both azimuth and range, by comparing the magnitude images. The differential interferogram is then created by subtracting the two interferogram phase components. Furthermore, a least-square best linear trend in azimuth and range is removed from the differential phase to account for first order residual orbit data inaccuracies and atmospheric heterogeneities. The linear trend removed varied from 0.0 to 0.5 radians over a 10 km scene. The resulting differential interferogram phase shown in Figure 3.

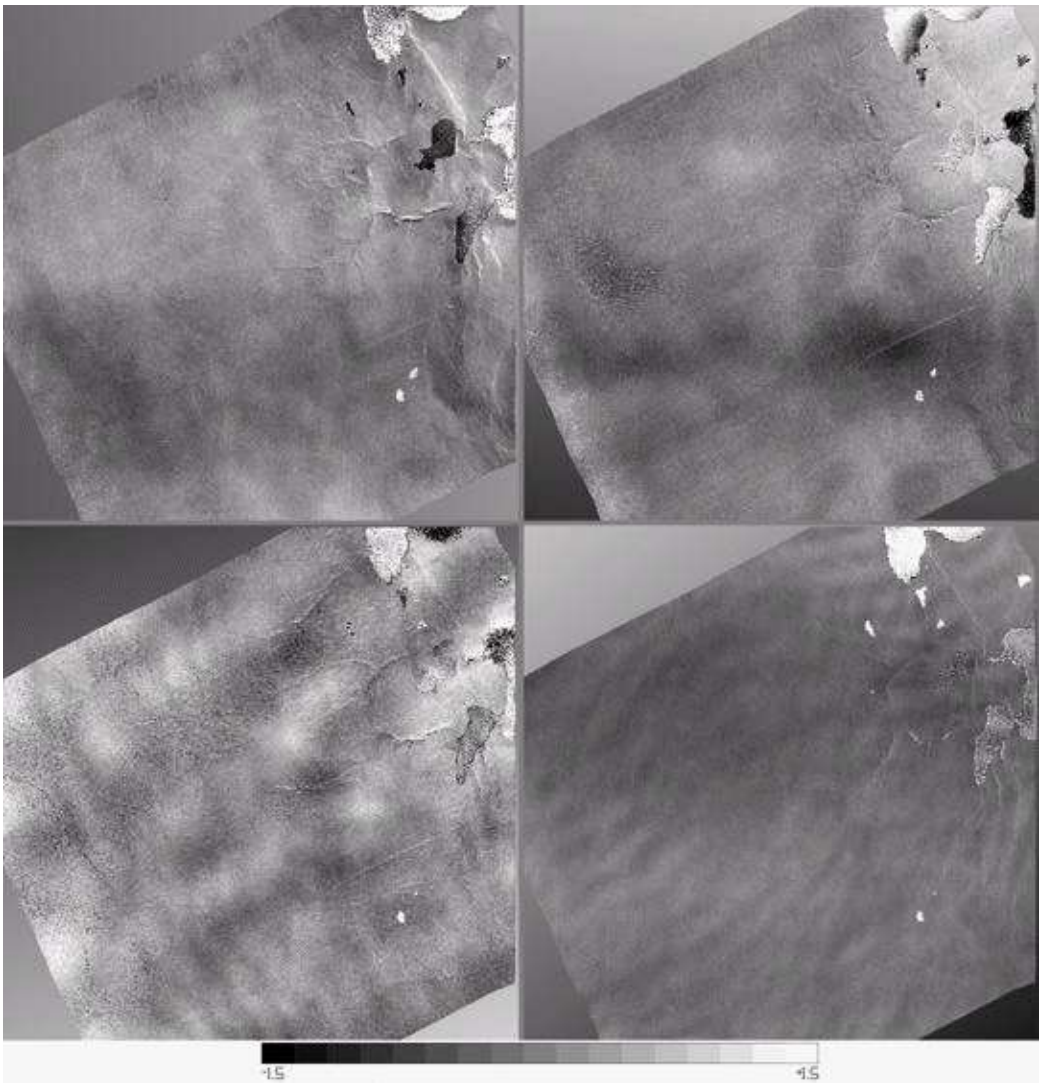

Figure 3: Set of differential interferograms from the ERS tandem mode data of Bathurst Island. The time sequence is from upper left to lower right and follows the sequence in Table 1. In each case a linear shift was applied in both the azimuth and range directions. The phase spans from -1.5 to +1.5 radians.

The residual phase shown in Figure 3, showing at times a wavelike pattern, has a peak to peak amplitude of approximately 1 radian with RMS values in uniform areas between 0.13 and 0.25 radians. Even in the case of the largest tandem baseline, an error of more than 50 m in the DTM would be necessary to account for this residual phase. This discounts ϕ_{top} as the main source of the discrepancy. A displacement of approximately 0.5 cm would cause a phase change of 1 radian. This also seems unlikely to be the principal source of the discrepancy since the pattern of the residual phase is very different in the four cases, and does not

correlate with geologic or land formations on the ground. And since ϕ_{noise} is a uniform noise component, we conclude that

atmospheric effects are the main source of the observed residual phase. The irregular wavelike pattern in the March 13 data (lower left panel) with spacial scale approximately 3 km in wavelength is characteristic of atmospheric effects. Others have also observed similar atmospheric effects in the order of 0.5 to 2 radians (Van der Kooij et al., 1995; Tarayre et al., 1996; Zebker et al., 1996).

The ever present possibility of substantial atmospheric component to the interferogram phase has implications for the use of repeat pass satellite interferometry for both DEM generation and displacement measurements. In the former case, choosing a large baseline (under the constraints imposed by scene decorrelation), enables the minimisation of ϕ_{atm} with respect to Δh,

thereby reducing the atmospheric component to a small fraction of the topographic component. However the slant range term, R, in the topographic component (equation 2) may also be affected by extraneous atmospheric delays and refraction. The use of a `fictive', an effective zero index of refraction, satellite position generated with the use of ground control points can be used to minimise pixel misregistration and residual atmospheric errors (Tarayre et al., 1994).

Unfortunately this flexibility is not available when using interferometry for displacement measurements. Furthermore the unpredictable nature of these effects makes it difficult to subtract them out with use of control points. The effect can be reduced by averaging a number of independent measurements, or when measuring displacements that are large with respect to nominal atmospheric effects.

3. GLACIER EXPERIMENT

The Saskatchewan glacier was the focus of a previous study where 5 ascending ERS tandem passes were used to estimate the flow field of the glacier (Vachon et al., 1996). We now expand the study, and seek to improve the estimate of the flow field by using both ascending and descending ERS tandem passes. The same procedure listed above is used to generate the interferogram and scene coherence. A representative tandem mode interferogram from November 2/3, 1995 is shown in Figure 4. The top two panels represent the interferogram magnitude and scene coherence. The lower panels represent the raw and flat-earth corrected phase, in both cases wrapped in intervals of 2. From the top we see Dome, Athabasca, and Saskatchewan glaciers. Among all the ERS tandem passes available only five ascending passes and four descending passes had sufficient coherence over the Saskatchewan glacier to be of use. These are listed in Tables 2 and 3 respectively.

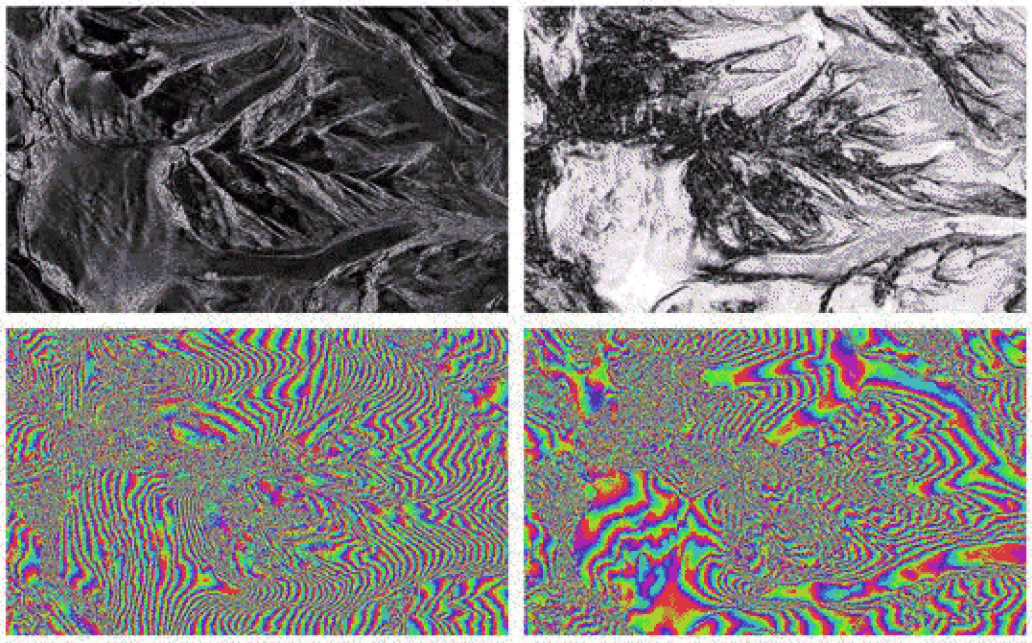

Figure 4: Representative tandem mode interferogram from November 2/3, 1995: interferogram magnitude (upper-left); scene coherence (upper-right); raw phase (lower-left); flat-earth corrected phase (lower-right). Each colour cycle in the lower panels represents a 2 phase change. Saskatchewan is the lower glacier.

Pass Date	Orbit	R.O.	B_n (m)
2/3 Nov 1995	22481/2808	449	94
21/22 Nov 1995	22753/3080	220	17
5/6 Mar 1996	24256/4583	220	245
21/22 Mar 1996	24485/4812	449	297
25/26 Apr 1996	24986/5313	449	34

Table 2: Summary of coherent ERS-1/2 ascending passes over Saskatchewan glacier

Pass Date	Orbit	R.O.	B_n (m)
26/27 Nov 1995	22832/3159	299	115
31/1 Dec/Jan '95/6	23333/3660	299	175
10/11 Mar 1996	24335/4662	299	27
29/30 Mar 1996	24607/4934	70	97

Table 3: Summary of coherent ERS-1/2 descending passes over Saskatchewan glacier

The differential interferogram is created as described in the previous section using an accurate DEM obtained from the CV-580 InSAR system (Figure 5) and PRC data from D-PAF. The differential interferograms were unwrapped, converted to line-of-sight displacement (LOS) using equation (3), and mapped back to UTM co-ordinates. Figure 6 and 7 show the LOS displacement *R* along the centrelines of the glacier for the ascending and descending Tandem passes respectively. Unlike the differential interferograms in the previous section, the difficult terrain in this case did not permit the removal of the best linear fit from this data set.

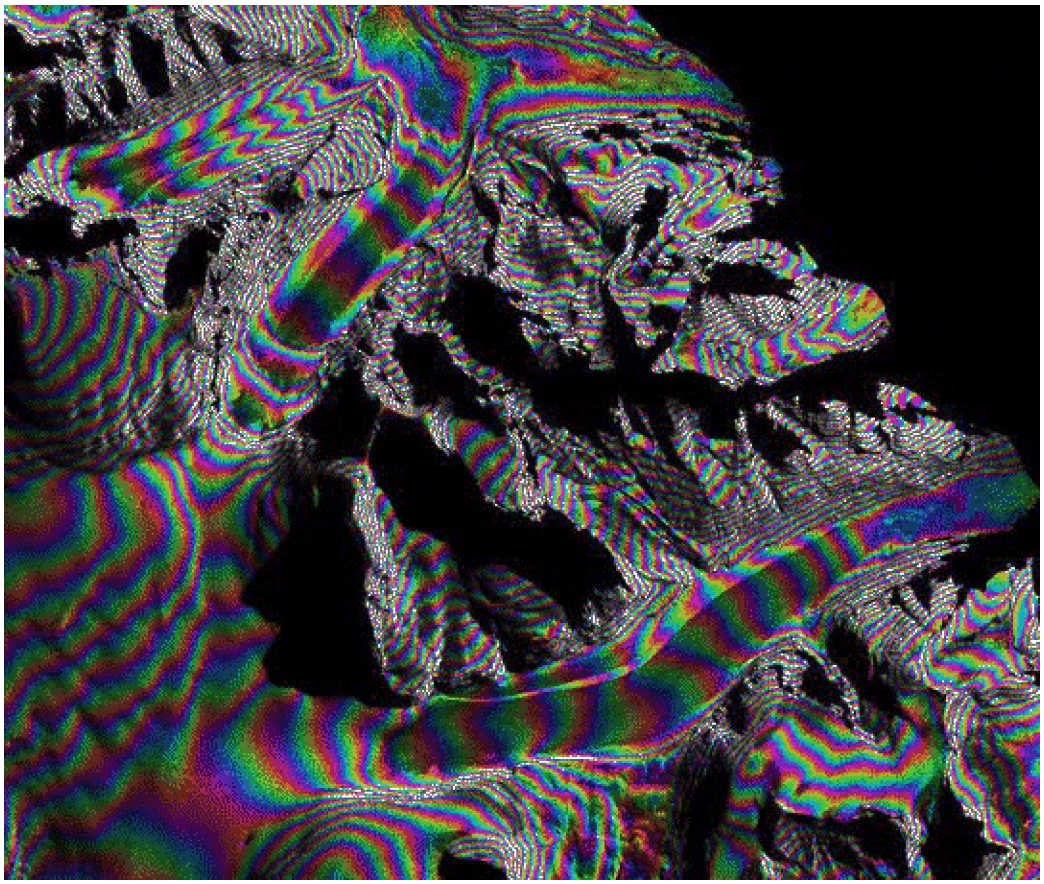

Figure 5: CV-580 cross-track InSAR-derived DEM from the Saskatchewan Glacier (bottom) and area, merged with the SAR image intensity. The map covers 13.5 km easting by 14.5 km northing. Each colour cycle represents a 50 m change in elevation. The data were acquired on March 25, 1995.

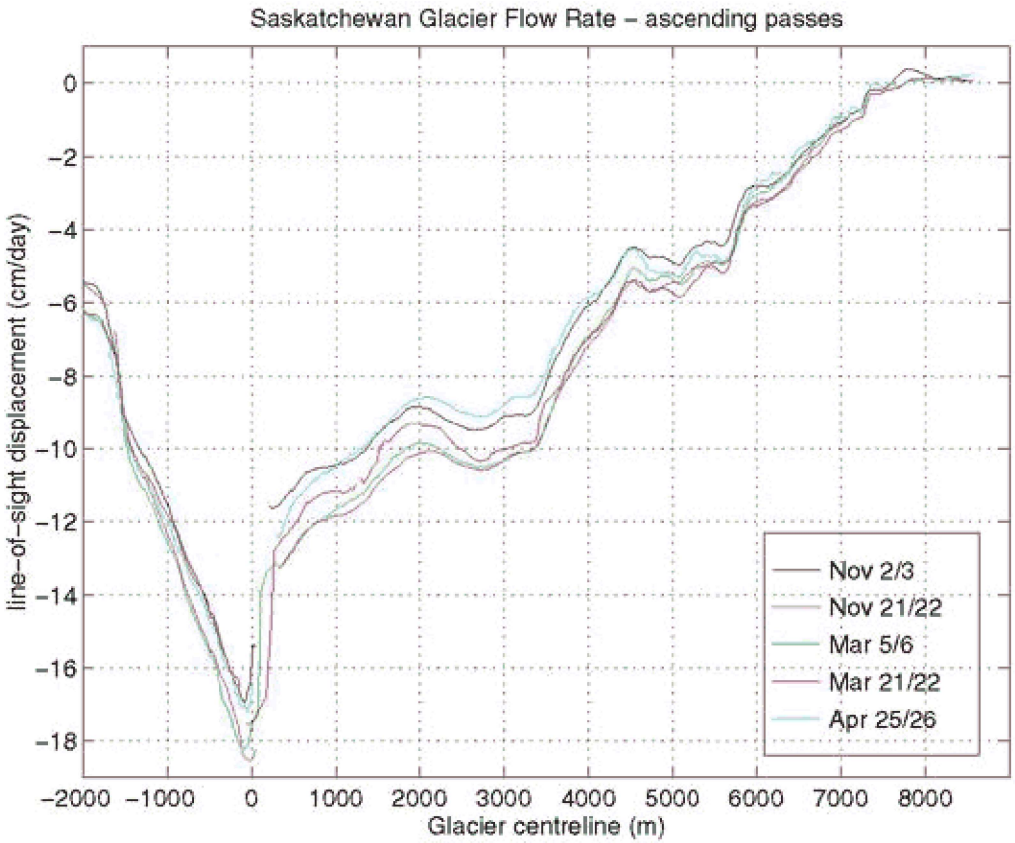

Figure 6: Plot of line-of-sight displacement derived from the differential interferograms of the ascending passes along the glacier centreline.

There may, therefore, be a linear trend in azimuth and/or in range. Without any other means of monitoring the atmosphere, there may be an atmospheric phase component as well. From the previous section, the linear trend could amount to up to 0.5 radians or

0.25 cm LOS over the scene, and the atmospheric phase component could be on the order of a radian, or 0.5 cm LOS. We cannot, therefore, rule out the possibility that the differences observed in the various ascending and descending LOS displacements in Figures 6 and 7 could be due to linear offset or atmospheric effects rather than real differences in the LOS displacement on the various dates. Nevertheless, these differences are small compared to the overall displacement observed.

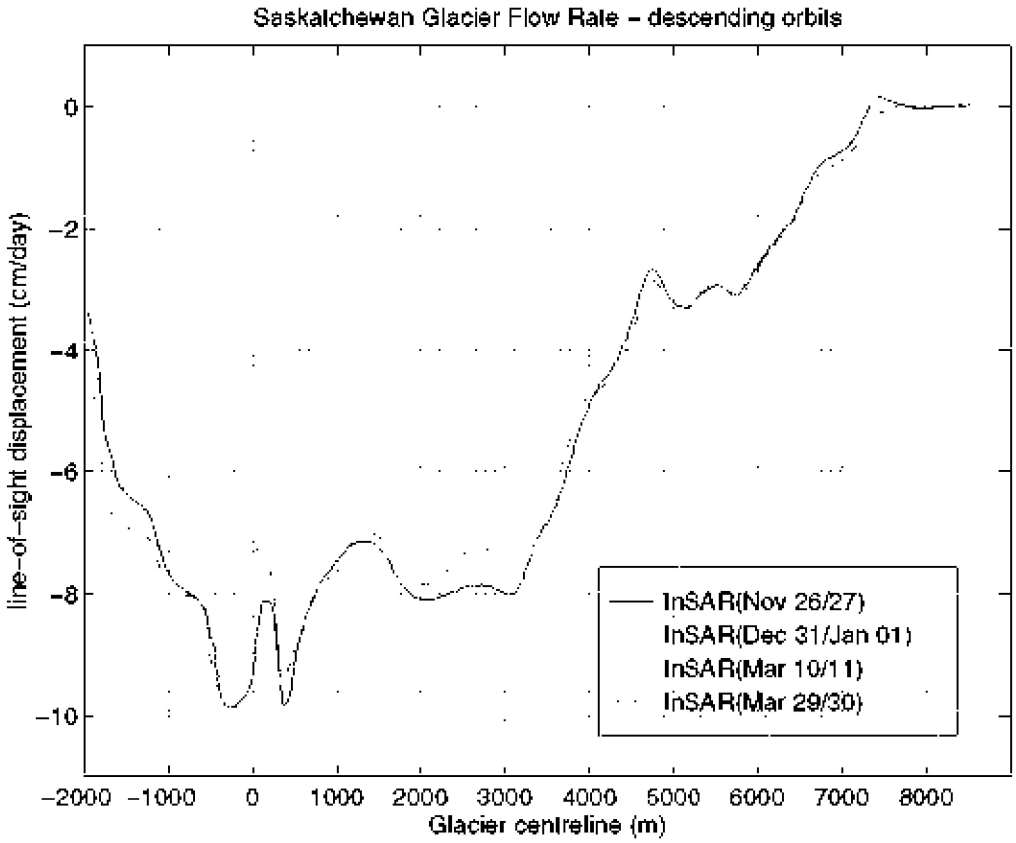

Figure 7: Plot of line-of-sight displacement derived from the differential interferograms of the descending passes along the glacier centreline.

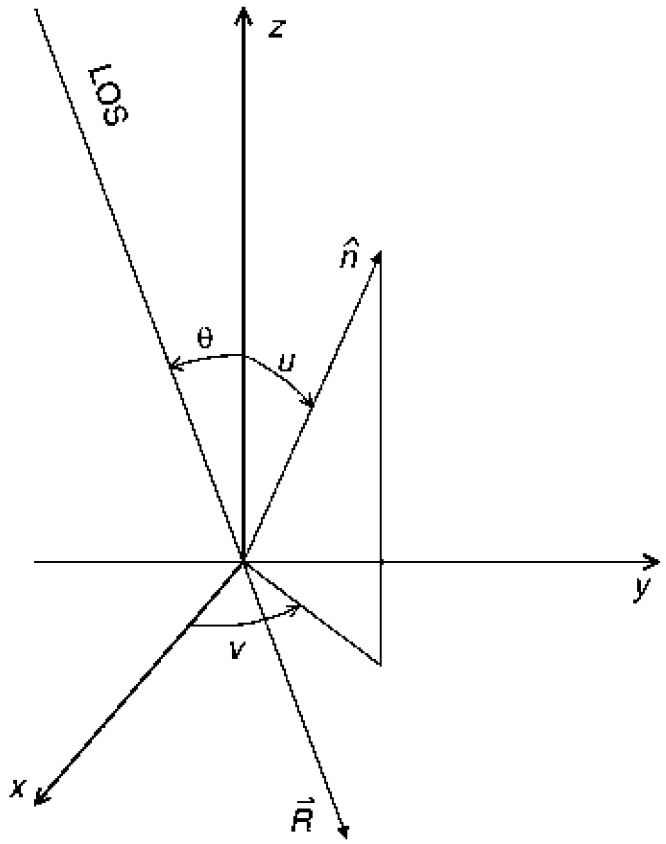

Figure 8: Diagram showing the surface normal geometry n and defining the angles u (surface slope) and v; $0u<180^o$; $-180^ov<180^o$. x is azimuth, y is range, and z vertical. The measured differential displacement R is in the direction of the radar line-of-sight. The incidence angle is measured with respect to local vertical and is positive for left-looking and negative for right-looking radars.

For the calculation of the surface displacement field we choose to use the March 5/6 LOS displacement from the ascending pass and the March 10/11 LOS displacement for the descending pass. They are closely spaced in time. They also have an average trend compared to the other ascending and descending passes.

The surface displacement field is measured by the repeat pass interferometry as projected along the radar LOS *R*. The surface displacement is given as (Vachon et al., 1996):

$$D = \Delta R / |\sin u \sin v \cos\phi + \cos u \sin\phi| \quad (4)$$

The geometry is shown in Figure 8. *u* is the angle between the vertical and local surface normal (varying between 0^o and 180^o), and *v* is the angle between x axis and the projection of the local surface normal on to the horizontal (varying between 0^o and 90^o).

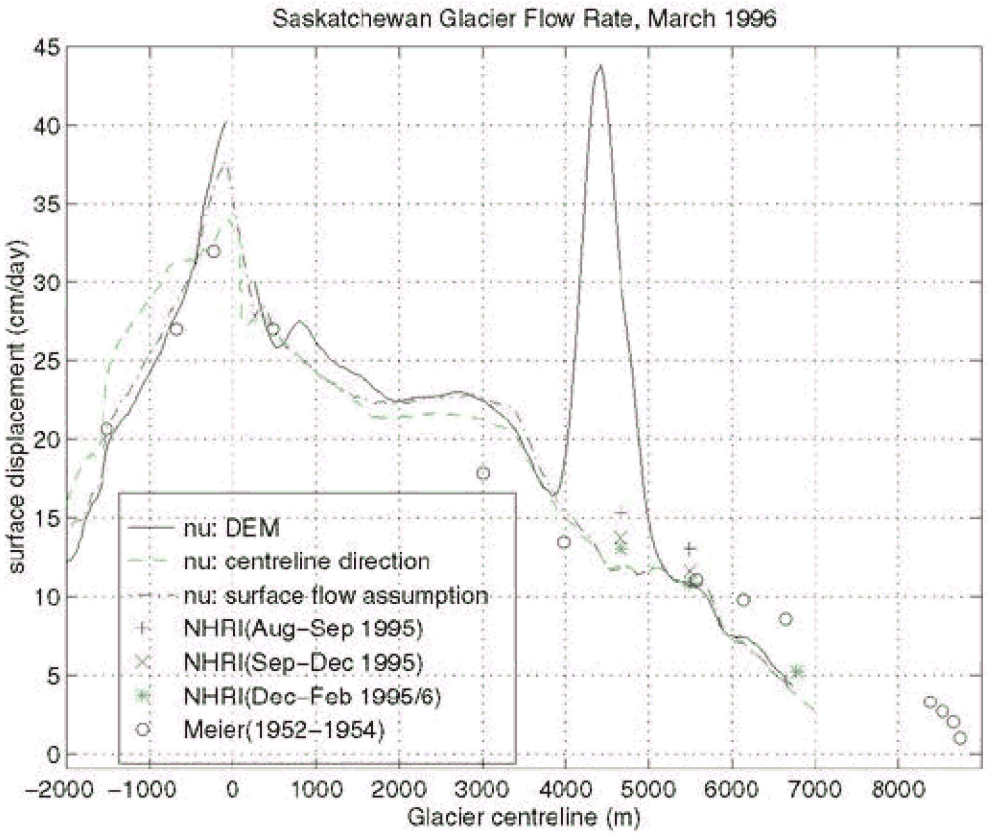

Figure 9: Plot of the downslope velocity using both the ascending and descending LOS displacement from the differential interferograms along the glacier centreline. Historic and recent surveying measurements are included.

Equation (4) has three unknowns: D, *u* and *v*. Since we have available both the ascending and descending LOS displacements, we can use equation (4) twice. We still need an assumption to solve for the displacement D. At least three different assumptions can be considered: (1) if the glacier flows in the direction of greatest slope, *v* can be calculated from the DEM. (2) *v* can be calculated assuming the flow is in the direction of the glacier centreline. (3) assuming the glacier flows parallel to the glacier surface $z_t(x,y)$, then the vertical velocity is related to the horizontal velocity by (Joughin et al., 1996):

$$v_z = [\nabla_{xy} z_t(x,y)]^T v_h \quad (5)$$

Equation (5) can then be used in combination with equation (4) to solve the D. Figure 9 is a plot of the displacement derived using each of these three assumptions. Also included in Figure 9 are historic and recent glacier flow measurements obtained the traditional (and very time consuming) triangulation method.

Each of the assumptions have their disadvantage. Assumption (1) obviously fails near the 4500 mark. This coincides with the area near the bend in the glacier where glacier *v* reaches nearly 70^o. The glacier is moving in the direction of the glacier centreline rather than in the direction of greatest downslope gradient. Assumption (3) applies only in portions of the glacier at steady state. It fails in regions of accumulation or ablation, where the flow is no longer parallel to the surface (Joughin et al., 1996). Nevertheless, it appears to be the best assumption of the three.

4. CONCLUSION

The Bathurst Island ERS tandem mode data shows that even in Arctic terrain under winter conditions there are atmospheric conditions which will affect radar wave propagation. The resulting interferogram differential phase from the combination of a pair of passes will have fluctuations of magnitude 1 to 2 radians due to these propagation anisotropies.. With a small baseline, as was obtained with the tandem mode data, this means that topographic information can be in error by many tens of metres. However, if the baseline is much larger (as has been obtained with RADARSAT fine mode data pairs) and with use of ground control points to create fictive satellite positions, the error from this source can be reduced to less than 10 meters.

In the Saskatchewan Glacier movement experiment the combination of data from both ascending and descending passes has helped address the problem of which assumption to make in converting a line-of-sight displacement to a glacier flow field.

5. ACKNOWLEDGEMENTS

ESA provided the ERS SAR data and D-PAF (GFZ Potsdam) provided the ERS orbit data. We thank M. Brugman (Columbia Mountains Institute of Applied Ecology), I. Cumming (UBC/EE), and J.-L. Valero (UBC/EE) for their contribution to the Saskatchewan Glacier study. G.D.'s contribution to this work was supported by an ESA fellowship.

6. REFERENCES

Geudtner, D.
"The interferometric processing of ERS-1 SAR data," Technical Report ERS-TT-1341 (Technical Translation of DLR-FB-95-28), ERA-ESRIN, European Aerospace Database, Frascati, Italy.

Geudtner D., M. Schwäbisch
"An Algorythm for precise reconstruction of InSAR imaging geometry," *Proceedings, EUSAR '96*, March 26-28, Königswinter, Germany, pp. 249-252.

Joughin, I., R. Kowk, R. Fahnestock
"Interferometric estimation of the three-dimensional ice-flow velocity vector using ascending and descending passes," submitted 1996, *IEEE GRS*.

Massmann, F.-H., Ch. Reigber, R. König, J.C. Raimondo, C. Rajasenan
"ERS-1 orbit information provided by D-PAF," *Proceedings, 2nd ERS-1 Symposium - Space at the Service of our Environment*, Hamburg, Germany, ESA SP-361, pp. 765-770, October 11-14, 1993.

Mattar, K.E., A.L. Gray, M.W.A. van der Kooij, P.J. Farris-Manning
"Airborne interferometric SAR results from mountainous and glacial terrain," *IGARSS*, pp. 1388-1390, 1994.

Tarayre, H. D. Massonnet
"Effects of a refractive atmosphere on interferometric processing," *IGARSS* pp. 717-719, 1994,

Tarayre, H., D. Massonnet
"Atmospheric propagation heterogeneities revealed by ERS-1 interferometry," *Geophysical Research Letters*, vol 23, no. 9, pp. 989-992, May 1, 1996

Vachon P.W., D. Geudtner, K. Mattar, A.L. Gray, M. Brugman, I. Cumming
"Differential SAR interferometry measurements of Athabasca and Saskatchewan glacier flow rate," *Can. Jour. Rem. Sens.*, vol 22, no. 3, pp. 287-296, September, 1996.

Van der Kooij, M., W. Groenwoud, B.A.C. Abrosius, G.J.Mets, B. Overgaauw, P.N.A. Visser
"Satellite radar measurements for land subsidence detection, " Land Subsidence, Barends, Brouwer & Schröder (eds), 1995.

Zebker, H.A., P.A. Rosen
"Atmospheric Artifacts in interferometric SAR surface deformation and topographic maps," submitted 1996*, J. Geophys. Res - Solid Earth*.

[1] Under contract from Intermap at CCRS.

[2] Now working at DLR, Institute of Radio Frequency Technology.

Keywords: ESA European Space Agency - Agence spatiale europeenne, observation de la terre, earth observation, satellite remote sensing, teledetection, geophysique, altimetrie, radar, chimique atmospherique, geophysics, altimetry, radar, atmospheric chemistry